ACS OMEGA

http://pubs.acs.org/journal/acsodf

Article

Effect of Infill Patterns with Machine Learning Techniques on the Tensile Properties of Polylactic Acid-Based Ceramic Materials with Fused Filament Fabrication

Ranganath Lolla, Adusumilli Srinath, Murali Govindarajan,* Manickam Murugan, Elumalai Perumal Venkatesan,* and Nasim Hasan*

Cite This: *ACS Omega* 2023, 8, 24786−24796

Read Online

ACCESS | Metrics & More | Article Recommendations

ABSTRACT: The field of additive manufacturing is quickly evolving from prototyping to manufacturing. Researchers are looking for the best parameters to boost mechanical strength as the demand for three-dimensional (3D) printers grows. The goal of this research is to find the best infill pattern settings for a polylactic acid (PLA)-based ceramic material with a universal testing machine; the impact of significant printing considerations was investigated. An X-ray diffractometer and energy-dispersive X-ray spectroscopy with an attachment of scanning electron microscopy were used to investigate the crystalline structure and microstructure of PLA-based ceramic materials. Tensile testing of PLA-based ceramics using a dog bone specimen was printed with various patterns, as per ASTM D638-10. The cross pattern had a high strength of 16.944 MPa, while the tri-hexagon had a peak intensity of 16.108 MPa. Cross3D and cubic subdivisions have values of 4.802 and 4.803 MPa, respectively. Incorporating the machine learning concepts in this context is to predict the optimal infill pattern for robust strength and other mechanical properties of the PLA-based ceramic model. It helps to rally the precision and efficacy of the procedure by automating the job that would entail substantial physical effort. Implementing the machine learning technique to this work produced the output as cross and tri-hexagon are the efficient ones out of the 13 patterns compared.

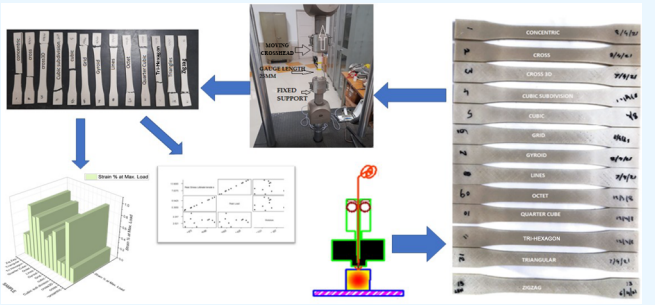

1. INTRODUCTION

Additive manufacturing, often known as three-dimensional (3D) printing, is a prototyping technique based on CAD (computer-aided design). A digital CAD file will be sliced and converted to a gcode form using a software, and the same will be printed layer by layer. Nonmetallic materials such as acrylonitrile butadiene styrene (ABS) and polylactic acid (PLA) are used. PLA is the most often utilized material due to its mechanical characteristics and light weight.[1] The benefits of additive manufacturing include cost savings, increased productivity, a shorter turnaround time, and customized output. Materials for the FFF (fused filament fabrication) method are restricted, and further study in this field is required. When comparing CNC (computer numerical control) and AM (additive manufacturing), CNC allows us to remove materials, whereas AM allows us to add to the fabrication. Dezaki and Mohd Ariffin[2,3] said that 3D printing is strong, is resistant to wear, corrosion, and oxidizing agents, and has good temperature resistance with a durable one.[4] In comparison to traditional manufacturing, FFF parts gave designers more freedom at a lower cost and weight. Internal parts, such as hollow shapes filled with solid infill matrices, might vary significantly during production. In a variety of sectors, AM technology is playing an increasingly important role in prototyping, pre-surgical models, and customized complicated designs. Its demand created opportunities for researchers and engineers to know the mechanical properties, material compositions, and behavior of materials to use a specific component or material to replace existing parts or components.

The AM process is divided into seven categories. The material extrusion (or FFF) process is the focus of this research. The goal of the project is to create a prosthetic hand for someone who is paralyzed or impaired. Before beginning any study, it is critical to choose the right materials and understand their qualities. A Mayo sensor that responds to the muscle movement in the body must control the prosthetic hand. Going a step further, if a disabled person utilizes this

Received: December 24, 2022
Accepted: May 15, 2023
Published: July 3, 2023

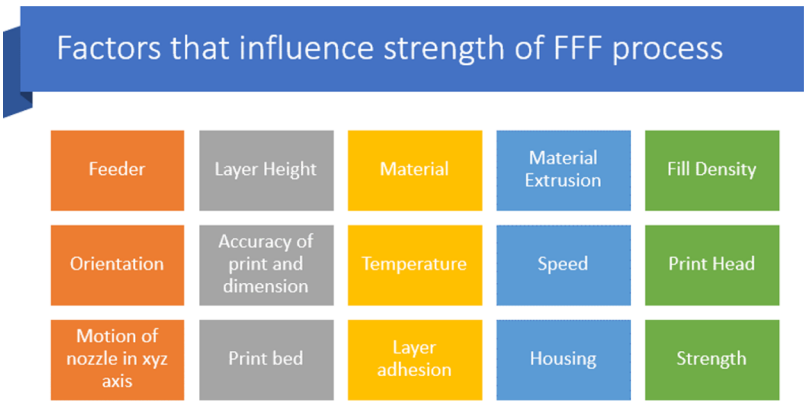

Figure 1. Factors that influence the strength of the FFF process.

artificially generated hand, he can employ straight insertion into the fractured area, not just for a paralyzed person. Biocompatibility, composition effect, characteristics, and availability are all requirements for this material. The chosen material must meet all the requirements. In this work, these factors are described and justified.

PLA-based ceramic was chosen as the process material. ABS (2% silicon carbide) is the material's composition. Silicon nitride (7% silicon), alumina zirconia (4% zirconia), 86% PLA, and 1% ABS were used (ABS stands for acrylonitrile butadiene sulfonate). The thermoplastic polymer styrene was also used. Gomes et al.[5] tested the biocompatibility and bioinertness of the ABS polyamide on rabbits. After studying the ABS-M30i biocompatible material, researchers found that it is bioinert.[6]

1.1. Literature Review. *1.1.1. Silicon Carbide.* Santavirta et al.[7] investigated silicon carbide (SiC) as a coating agent. SiC is a stiff substance made up of tightly packed molecules that are difficult to degrade. When comparing silicon carbide to hydroxyapatite, the same is true; both results exhibit the same qualities.[8] They determined that crystalline silicon carbide is biocompatible and hemocompatible as a result of their findings. It is the only semiconducting substance that possesses this feature.

1.1.2. Silicon Nitride. In his review, Heimann[9] determined that silicon nitride is a biomaterial that can replace titanium. It has applications in dentistry, orthopedics, prosthetics, cardiovascular surgery, and reconstructive surgery. When silicon nitride particles were compared to normal orthopedic biomaterials, no adverse reactions were observed in the donors; however, cobalt−chromium caused cytotoxicity.

1.1.3. Zirconia Alumina. Maccauro et al.[10] investigated the properties of zirconia and alumina in vitro and concluded that when introduced into the human body, they had no harmful effects.

1.2. Playing Game. PLA and its copolymers have been proven to be biocompatible and safe in study papers for the past two decades.[11] However, the chemical mixture of other components necessitates consideration.

When combined with other substances, it can modify its chemical composition and cause toxicity. It is clear from the literature that all PLA-based ceramic materials are biocompatible. Aside from composition, another key topic to consider is printing process settings. Air gap, build orientation, extrusion temperature, infill density, infill pattern, layer thickness, print speed, raster width, and raster orientation were all explored in ref 12. When compared to other process parameters, the research gap revealed weak infill pattern, shell width, extrusion temperature, and print speed. Based on the conclusion statement, this work focused on the infill pattern and its effect on strength.

Different characteristics influence the strength of a 3D printed product. Stability is influenced by a variety of factors, including fill density, orientation, nozzle motion, print bed parameters, temperature, material, and many more, as shown in Figure 1. Strength is directly proportional to fill density; 100% infill density results in great strength. The temperature of the bed and nozzle varies according to the material being used. The bed temperature for PLA is 60 °C, while the nozzle temperature is 230 °C. The quality of the output is inversely proportional to the nozzle speed rate; feed rate maximum results in minimum quality output—printing orientation is another important process parameter. The easiest way to determine the layer height is to compare it to the nozzle diameter; the layer height should be between 25 and 75% of the nozzle diameter.

Using a combination of AM and investment casting techniques, the paper offers a study on the creation of a metal matrix composite using recycled resources.[13] The impact of various processing parameters on the microstructure and mechanical characteristics of the composite was examined by the authors. In comparison to the basic material, the created composite had better mechanical properties, according to the results, and the suggested method may offer a sustainable alternative for producing metal matrix composites.

A collection of studies on additive manufacturing and material properties are discussed in detail on the wear performance of ABS parts, weaving infill pattern inspection of oil distribution in different patterns, microstructures, and mechanical properties of various additive materials. These studies contribute to the advancement in the practices of additive manufacturing in different directions and processes.[14−26]

2. METHODOLOGY

It is necessary to understand the basic concept of the FFF process before delving into the process parameters. The layout of the FFF process is depicted in Figure 2a. The material is a filament that is fed via a heated nozzle. At the nozzle point, the material is heated to melting temperatures, and the fused material is deposited layer by layer on the bed. AM is the name for this method. The fused filament creation method is depicted in detail in Figure 2b.

https://doi.org/10.1021/acsomega.2c08164
ACS Omega 2023, 8, 24786−24796

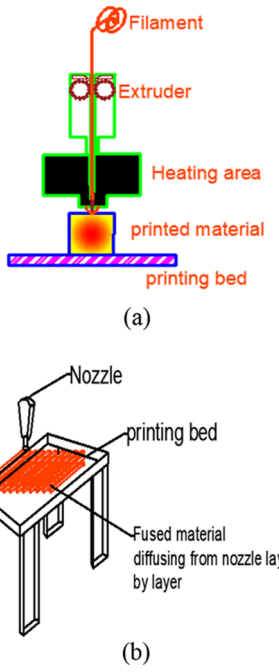

Figure 2. (a) Two-dimensional representation of the fused filament process. (b) Isometric view of the 3D printing process onto the bed.

The mechanical properties of the ceramic filament acquired from WOL3D were investigated, as well as the composition. The outcomes of the following are discussed. The 1 kg spool acquired from WOL3D (world of Lilliput's) looks similar to Figure 3. Figure 4 explains the steps involved in generating a

Figure 3. Material purchased from WOL3D.

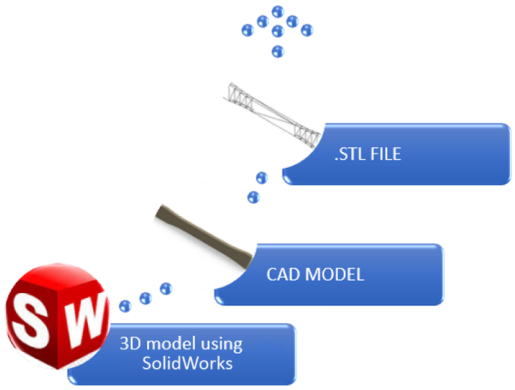

Figure 4. Procedure to generate the .stl file from the SolidWorks software.

.stl from a 3D model using SolidWorks software. They had a variety of filaments in various sizes, and they chose the ceramic filament as the basis for this project.

The output of a 3D printer is determined by the printing parameters, which necessitates certain methods, as shown in Figures 4 and 5. The first step is to create an ASTM D638-10

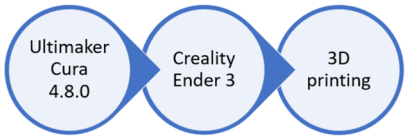

Figure 5. Exported .stl from SolidWorks imported to Ultimaker Cura, sliced, and printed in a Creality Ender machine.

dog bone specimen in SolidWorks. A 3D specimen model is created and then exported as a .stl (standard triangular language) file. The exported .stl file is then imported into Ultimaker Cura version 4.8.0, a slicing software. Table 1 shows

Table 1. Settings to Print Specimen

layer height		0.12 mm
wall thickness	wall thickness	1.2 mm
	wall line count	3
	top/bottom thickness	0.84 mm
	top layers	7
	bottom thickness	0.84 mm
	bottom layers	7
	horizontal expansion	0 mm
infill		20%
printing temperature		260 °C
build plate		100 °C
speed		50 mm/s
retraction	enabled	
fan speed		100%
support	nill	
build plate adhesion type	brim	

the slicing options and their settings. After that, it is converted to G-code and printed on a Creality Ender 3 machine. The parameters considered are print temperature, bed temperature, speed of the nozzle,[27] retraction, support, adhesion type, layer height, and fan speed, and the settings set in Cura stated in Figure 1 and discussed in Table 1.

Figure 6 explains the detailed process layout of the paper material selection, which was the first step, followed by studying and testing properties; the obtained results were analyzed using machine learning techniques; and based on the output results, the conclusion was framed.

3. EXPERIMENT

The focus of the project was on efficient infill patterns and material composition. The first half of the presentation covered material composition, while the second half concentrated on tensile testing and infill pattern mechanical properties. The crystalline structure and microstructure of the ceramic material were investigated using an X-ray diffractometer (XRD) and an EDAX with a scanning electron microscopy (SEM) attachment. The X-ray diffraction (XRD) patterns were recorded on the "PANalytical EMPYREAN diffractometer" using Cu K_α (λ = 1.5405 Å) radiation and EDAX performed with SEM from TESCAN. TESCAN is a manufacturing company of SEM. We discovered that the ceramic composition is amorphous, with few peaks appearing from the native components present in the copy, based on the XRD pattern. On average, EDAX could

https://doi.org/10.1021/acsomega.2c08164
ACS Omega 2023, 8, 24786−24796

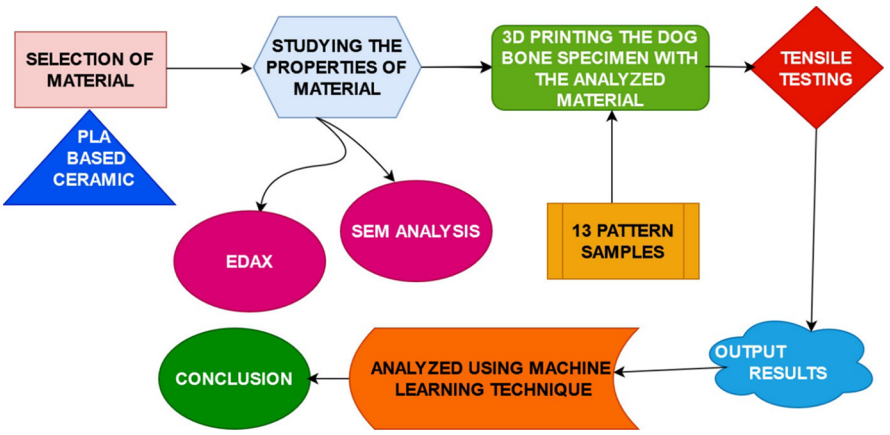

Figure 6. Algorithm for the proposed work.

calculate the percentage of features present and the elemental analysis at different locations. The results show that the composition is in perfect agreement with the outcomes. Figure 7 exhibits the ceramic filament pattern, which includes a few

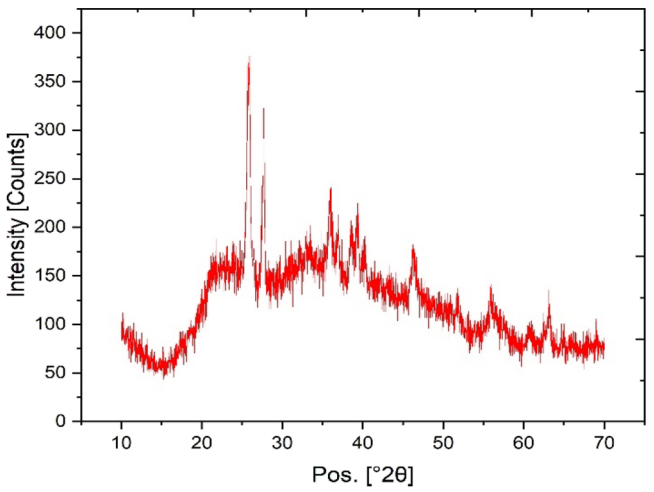

Figure 7. XRD pattern of the ceramic filament.

peaks from native elements, and Figure 8 depicts the EDAX results; after quantifying the other characteristics of the composition, it closely fits the chemical formula.

The formula for PLA is $(C3H402)n$. From EDAX measurements, referring to Figure 8, it is identified that carbon is around 58%, oxygen is about 41%, and the remaining elements are 1%. Even though PLA contains hydrogen, it is a low atomic number element. EDAX is unable to trace. When quantifying other aspects in the composition, it nicely matches with the given chemical formula.

3.1. Properties of PLA-Based Ceramic Materials as for Manufacturers' Data. The density is 1.26 g/cm^3, the tensile modulus is 2436.28 MPa, the thermal conductivity is 0.12 W/mK, the heat capacity is 1800 kgK, the heat deflection temperature is 46 °C, and the Poisson ratio is 0.3. The next part is to determine the printing properties, and that too with the infill pattern with which practice needs to print needs to be studied with experimental procedure and carried out below with the dog bone of dimensions shown in Figure 9a. A total of 13 samples of the dog bone specimen are printed with the dimension shown in Figure 9b. And also, the printed samples

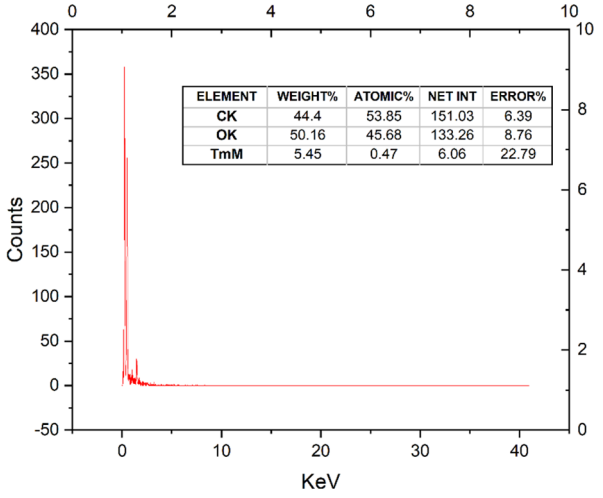

Figure 8. EDAX result for the ceramic filament.

with numbers mentioned are sample 1, concentric; sample 2, cross; sample 3, cross3D; sample 4, cubic subdivision; sample 5, cubic; sample 6, grid; sample 7, gyroid; sample 8, lines; sample 9, octet; sample 10, quarter cube; sample 11, tri-hexagon; sample 12, triangular; and sample 13, zigzag. The shapes of these patterns are illustrated in Figure 10.

The above tabular data signifies the slicing settings of Ultimaker Cura software. The layer height decides the quality of the product. In Cura, 0.12 mm represents superquality; 0.16, dynamic quality; 0.2, standard qualities; and 0.28, low quality. For the specimen printed 0.12 mm, i.e., the superquality option is selected. The wall thickness options are not touched up; those are kept as it was. The infill percentage is another research concentric area, and researchers are studying by varying infill percentages like 10, 20, 30, 40 up to 100.[28]

Nevertheless, for this experimental condition, 20% infill is considered. The printing temperatures of both the nozzle and bed are 200 and 100 °C, respectively. The manufacture specifies these temperatures in the range of 200−240 and 60−100 °C, respectively. The nozzle speed was maintained at 50 mm/s; this consideration took based on the trial-and-error method; 100 mm/s will give poor output. Retraction enabled to the design retraction will not be having much effect because the shape is not complex. Support is not needed as there is no hanging part in the model. Finally, the adhesion type option brim is selected. The skirt will not lay a layer on the bottom;

https://doi.org/10.1021/acsomega.2c08164
ACS Omega 2023, 8, 24786−24796

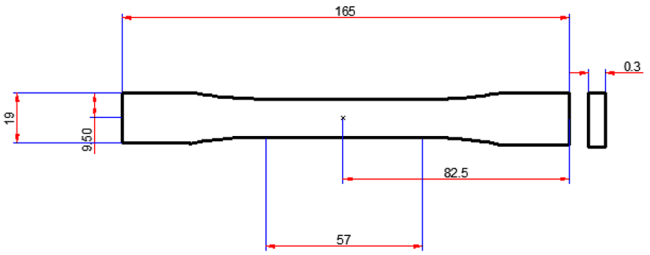

(a)

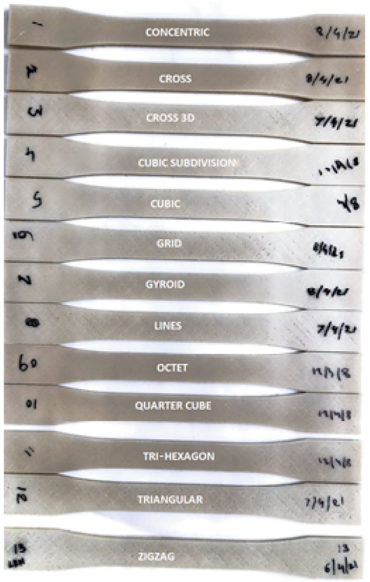

(b)

Figure 9. (a) Dog bone dimensional parameters carried out for testing. (b) Series of samples printed using Ultimaker Cura 4.8.0 with standard dimensions as shown above.

the raft option consumes more than brim; brim is the perfect choice for the above case. With all the said options, the 13 samples were printed, as shown in Figure 9. Figure 10 illustrates the various patterns printed that are obtained after slicing in Ultimaker Cura software, as suggested in refs 29−31. Table 2 gives information on the material used in grams and meters and time taken for every sample. Though the patterns

Table 2. Pattern Printing Time and Material Consumption

s. no.	pattern type	time (h.min)	grams	meters
1	concentric	1.22	7	2.28
2	cross	1.28	7	2.33
3	cross3D	1.28	7	2.33
4	cubic subdivision	1.23	7	2.27
5	cubic	1.24	7	2.33
6	grid	1.23	7	2.32
7	gyroid	1.25	7	2.33
8	lines	1.24	7	2.32
9	octet	1.24	7	2.33
10	quarter cubic	1.24	7	2.33
11	tri-hexagon	1.24	7	2.32
12	triangles	1.24	7	2.32
13	zigzag	1.24	7	2.36

are different, it is evident that 7 g of the material is used for all 13 samples. Zigzag used 2.36 m as maximum and 2.26 cubic subdivision records for low consumption in terms of meters. Cross and cross3D took a little extra time, like 6 s extra, compared to other samples. Concentric printed in 1.22, i.e., 1 h 22 min. The average time to print each sample is 1 h 24 min.

The printed samples are loaded in a nano-universal testing machine (UTM), as shown in Figure 11. Figure 12 depicts the

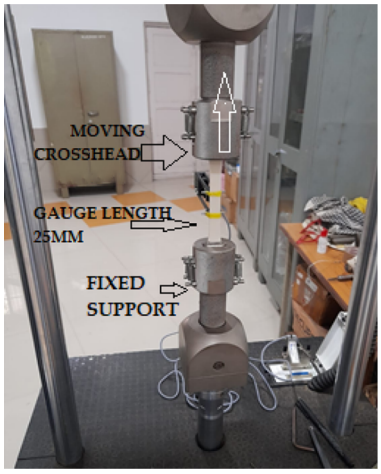

Figure 11. Tensile testing of specimen nano-UTM.

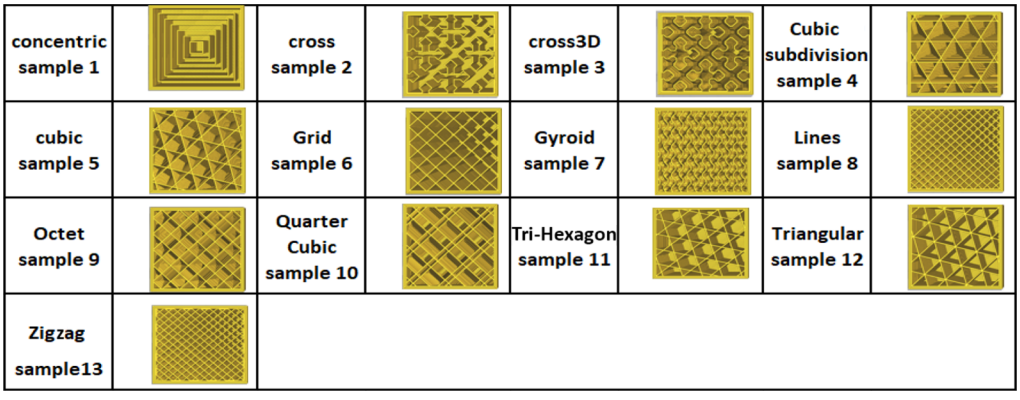

Figure 10. Patterns printed obtained after slicing in Ultimaker Cura software.

https://doi.org/10.1021/acsomega.2c08164
ACS Omega 2023, 8, 24786−24796

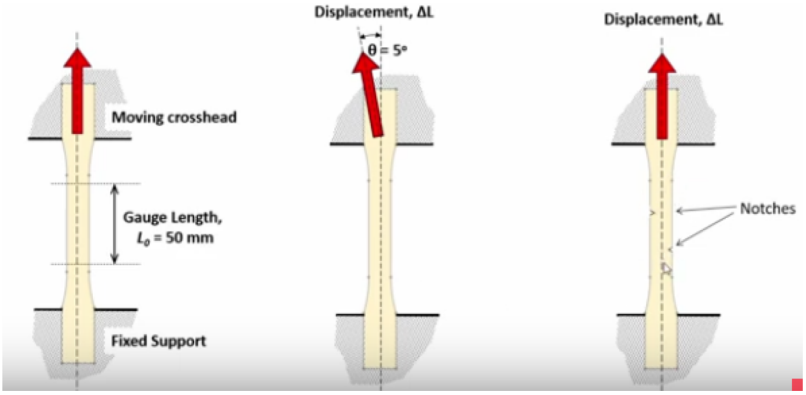

Figure 12. Standard way to keep the specimen and possible errors during the setup formula.

standard way to keep a specimen inside the UTM machine; results will vary with an alignment error, as per the suggestion given in ref 32. The Notch area is also highlighted in Figure 12. The gauge length for the sample was considered (25 mm). The bottom crosshead is fixed, the upper crosshead is moved, and the specimen operates in between crossheads. Too much tightening the crosshead results in different damage patterns, and those cases are discussed in Results and Discussion.

4. RESULTS AND DISCUSSION

The process of AM is existing in every field. FFF is the most common process used in many sectors because of its economic conditions and easy handling. In addition, the raw materials (thermoplastics and composite materials) are abundant in availability and inexpensive. All these reasons made this process use in every industry. Though the application of this technology has an enormous benefit, the problems faced by these sorts of prints are also of the same kind.

The peak stress recorded for the cross is 16.944 MPa, and for tri-hexagon, it is 16.108 MPa; these are the patterns that show good results compared to other patterns. The values for cross3D and cubic subdivisions are 4.802 and 4.803, respectively; these are in the bottom rows of the table. Figure 13[33] depicts the specimens after tensile testing. It shows that

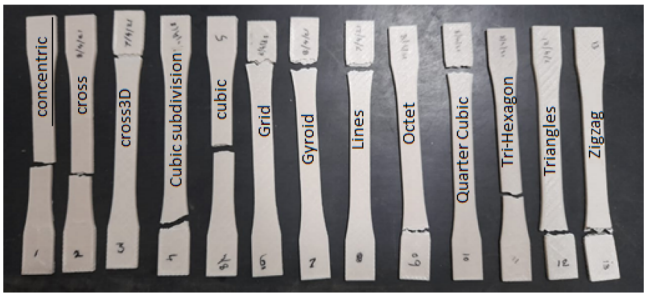

Figure 13. Specimen after testing.

almost all failed at the grip area, except four. The reasons for the above case are improper setup.[34] The angled failure of the specimen is due to anisotropic behavior, representing the polymer's composition having an indiscriminate alignment of fibers. The break at grip areas is due to a high clamping effect and lack of tabs. Excessive stress concentration at the grip areas results in the fracture at the grip. These can be overcome by adding a layer at the grip areas or providing the glue to the grip area, which will reduce the effect.[35]

$$\sigma = \frac{P}{wt}, \in = \frac{\Delta L}{L0}$$

$$K_{IC} = Y\sigma\sqrt{\pi a}$$

where Y is the dimensionless constant depending on the geometry, typically $Y \approx 1$; σ is the remote tensile strength; and a is the crack length.

Concentric and tri-hexagon are damaged in between because of the property. Figure 14 depicts the stress−strain curve for all

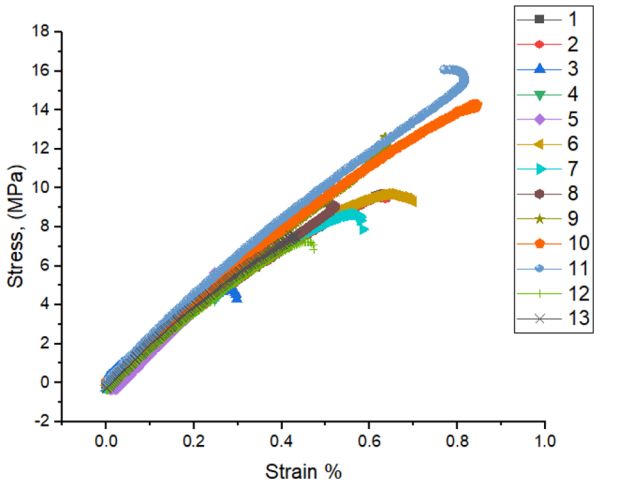

Figure 14. Stress−strain curve for all 13 samples of different infills.

13 patterns. They followed the path of polymer stress−strain. The graph shows that sample 2 (concentric) and sample 11 (tri-hexagonal) are recorded with peak values. Sample 3 (cross3D) and sample 4 (cubic subdivision) are recorded with the lowest strength regarding the graph data. The same data is plotted in the bar graph in Figure 15. The graph was plotted by taking samples on the x-axis and the ultimate tensile strength on the y-axis. The results show that concentric is having good strength out of all others and next in the list will be tri-hexagon.

The stress−strain curves for different samples and their results are available in refs 36 and 37.

Figure 16 illustrates the results plotted between the modulus and the infill.[38] Though the infill is standard of 20%, there is a slight variation in the effect of the modulus ranging from 1.902 to 2.374. The zigzag noted with 2.375 followed tri-hexagon and triangular. Figure 17 illustrates the max load with a strain, and they are indirectly proportional way. As the load increases, the

https://doi.org/10.1021/acsomega.2c08164
ACS Omega 2023, 8, 24786−24796

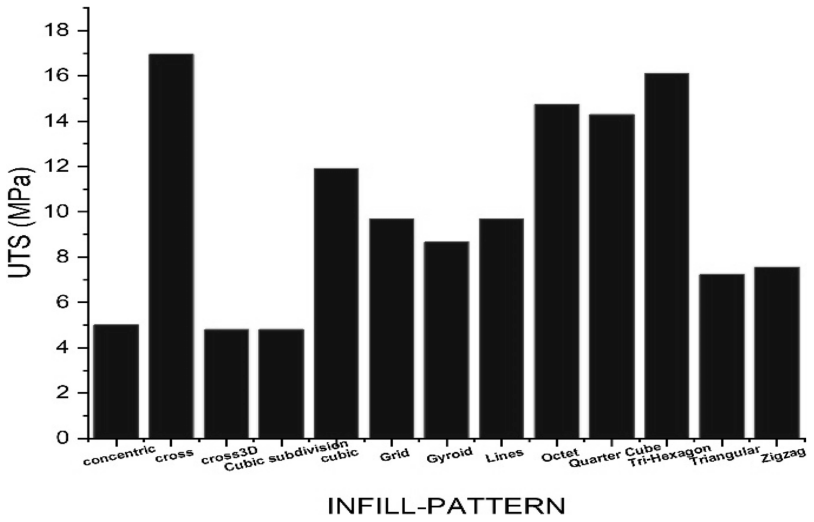

Figure 15. Ultimate tensile stress recorded for each sample.

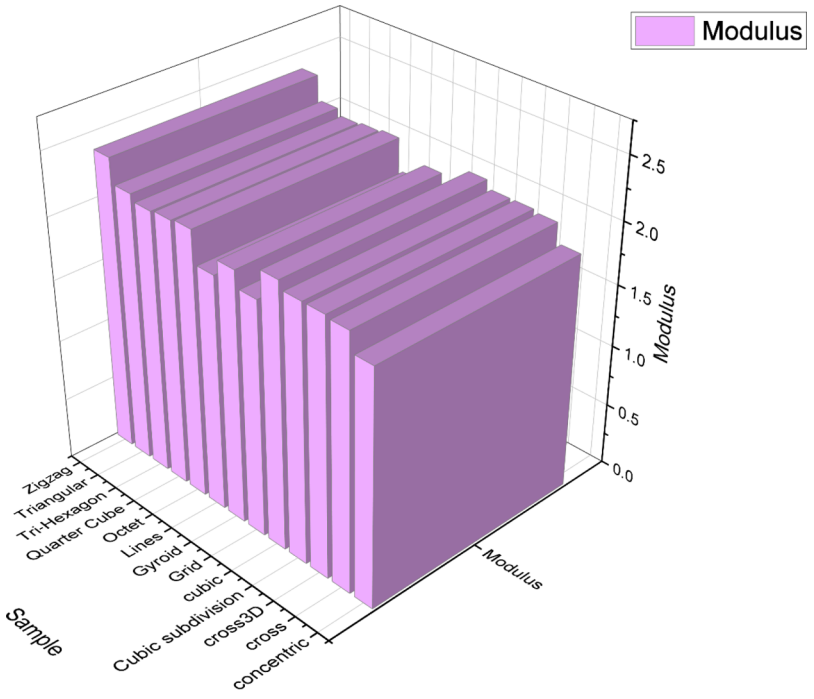

Figure 16. Infill 20% with a modulus value.

strain increases, and the max load and strain are recorded for sample 2 and sample 11, as discussed earlier in the previous graphs. Figure 18a,b shows the pattern shapes (concentric and tri-hexagon, respectively) after slicing the model in Ultimaker Cura software to understand the pattern structure better.

Before applying the machine learning technique,[39] let us check the normality of the data. If the data is not following the normality, then convert into normal through various transformation techniques.

Probability: All possible outcomes can be calculated with likelihood, which is what probability is. A random variable is defined by its thing of interest. The combination of probability with random variable, i.e., relation between conceivable outcomes for a random variable, is known as probability distribution.

Normal distribution: Same means and standard deviations are not necessary for normal distribution. Each set of data will be having its own data sets. Mean value "0" for normal distribution and "1" for standard deviation is known as Z-distribution.

$$Z = x - \frac{\mu}{\sigma}$$

where x is the standardized value, μ is the mean of the original distribution, and σ is the standard deviation.

Lognormally distributed

$$f(x) = e - \left(\frac{\left(\ln\left(\frac{x-\theta}{m}\right)\right)2}{2\sigma 2}\right)(x-\theta)\sigma 2\pi\sqrt{x} > \theta;\ m, \sigma > 0$$

Hazard function $h(x, \sigma) = (1x\sigma)\phi(\ \ln x\sigma)\Phi(\ -lnx\sigma)x > 0;\ \sigma > 0$

Survival function $S(x) = 1 - \Phi(\ln(x)\sigma)x \geq 0;\ \sigma > 0$

https://doi.org/10.1021/acsomega.2c08164
ACS Omega 2023, 8, 24786−24796

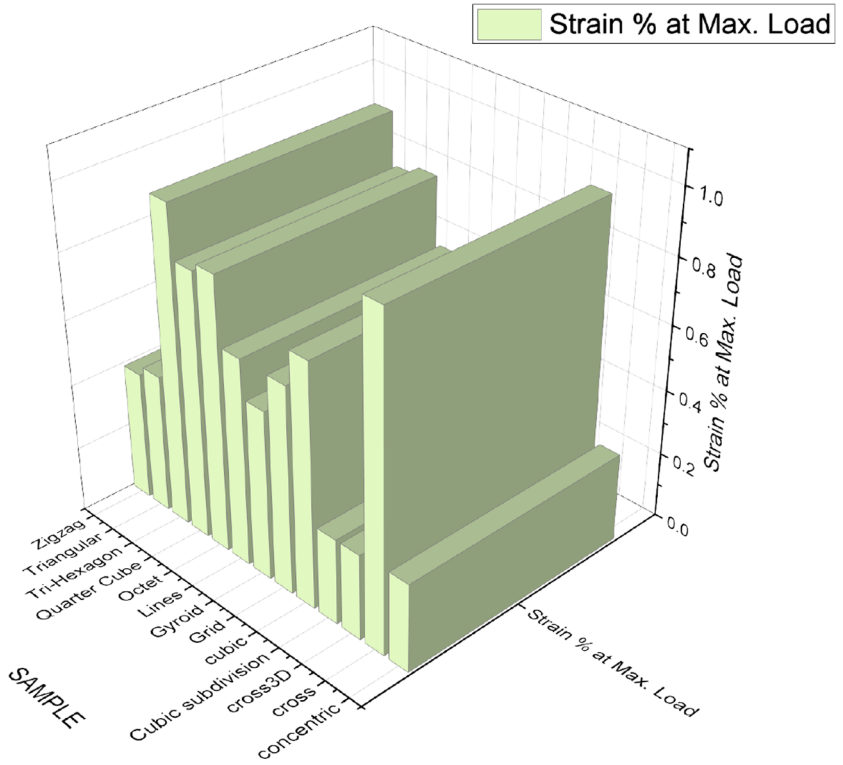

Figure 17. Strain % at max load with a funnel graph.

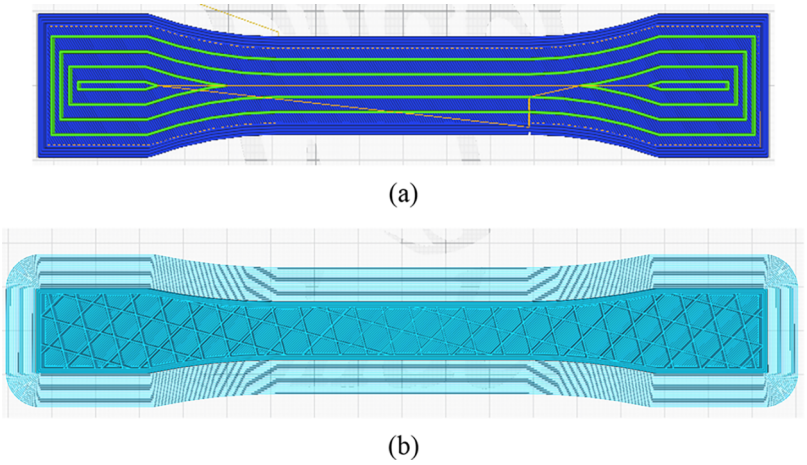

Figure 18. (a) Pattern after slicing the specimen in Ultimaker Cura software (concentric). (b) Pattern after slicing the specimen in Ultimaker Cura software (tri-hexagon).

$$\text{probability density } P(x) = \frac{1}{(\sqrt{((2\text{pi})x)}e^{-(\ln x - M)^2/2S^2})}$$

Figure 19 illustrates the impression of peak stress, peak load, and modulus.

Normality: Normality of the data have been verified for various distributions like normal, lognormal, Weibull, and exponential.

Lognormal: The lognormal distribution is generally employed to measure weakness-pressure on technical methods.

Weibull: To obtain failure rates, this Weibull is flexible. For distorted distributions, lognormal will be used to outmost. To take the natural log for a random variable results in normal distribution.

Figure 20 represents the relationship between the peak load and peak stress, peak load and modulus, and modulus and stress with the effect of the infill pattern and strength.[40]

Correlation: The intensity to which two variable quantities move in management with one another.

Matrix plot: Figure 21 depicts the matrix plot to find the relation between each of the variables.

5. CONCLUSIONS AND FUTURE SCOPE

The surface finish and mechanical properties of the product depend on the optimum arrangement of process parameters. Process parameters like infill patterns, raft angles, and nozzle temperature need a deep study of the individual material. This work focused on the infill pattern strength of a PLA-based ceramic filament purchased from the WOL3D website. The

https://doi.org/10.1021/acsomega.2c08164
ACS Omega 2023, 8, 24786−24796

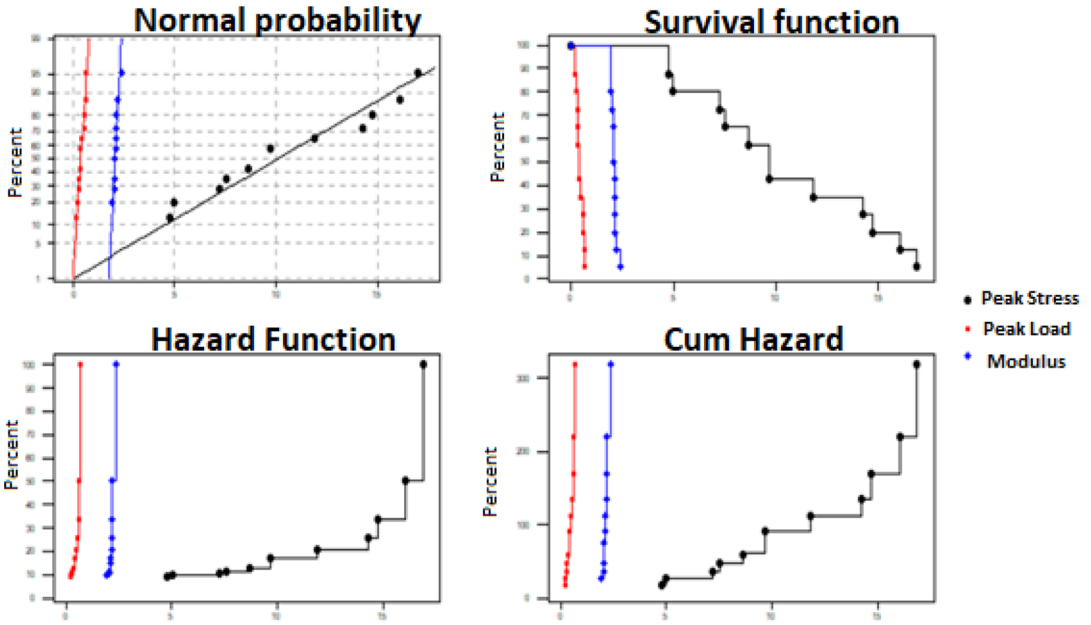

Figure 19. Overview plot for peak stress, peak load, and modulus.

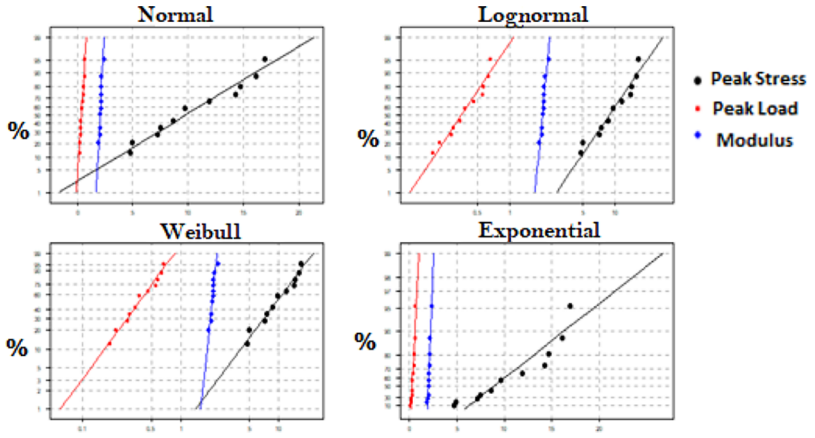

Figure 20. Four-way probability plot for peak stress, peak load, and modulus.

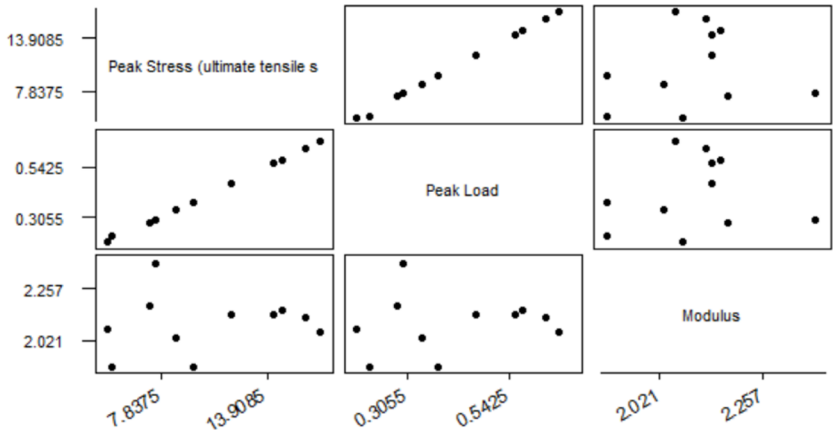

Figure 21. Matrix plot.

properties and different structural patterns are studied with 13 designs in number concentric, cross, cross3D, cubic subdivision, cubic, grid, gyroid, lines, octet, quarter cube, tri-hexagon, triangular, and zigzag. Out of all 13 designs, the efficient ones are cross and tri-hexagon, followed by an octet and quarter cube. Cross3D and cubic subdivisions are last on the list. The inference has done based on the peak stress and peak load data generated from tensile testing. Optimizing

https://doi.org/10.1021/acsomega.2c08164
ACS Omega 2023, 8, 24786−24796

parameters can reduce energy consumption in the printing process.[41]

Ceramic-based PLA properties in bioinertness need to be examined. Biocompatibility needs to be examined as per FDA norms and the toxic nature needs to be tested. PLA-based ceramic material hardness, fatigue, and other properties need to be tested. Finite element analyses need to be on the samples, and the test results need to be compared.

AUTHOR INFORMATION

Corresponding Authors

Murali Govindarajan − *Department of Mechanical Engineering, Koneru Lakshmaiah Education Foundation, Vijayawada, Andhra Pradesh 520002, India*; Email: muralinitt@gmail.com

Elumalai Perumal Venkatesan − *Department of Mechanical Engineering, Aditya Engineering College, Surampalem, Andhra Pradesh 533437, India*; orcid.org/0000-0002-7536-8200; Email: elumalaimech89@gmail.com

Nasim Hasan − *Department of Mechanical Engineering, Mechanical Engineering, Mattu University, Metu 524413, Ethiopia*; orcid.org/0000-0002-4718-2767; Email: nasim.hasan@meu.edu.et

Authors

Ranganath Lolla − *Research Scholar, Department of Mechanical Engineering, Koneru Lakshmaiah Education Foundation, Vijayawada, A.P. 520002, India*

Adusumilli Srinath − *Department of Mechanical Engineering, Principal of Academics staff college, Koneru Lakshmaiah Education Foundation, Vijayawada, A.P. 520002, India*

Manickam Murugan − *Department of Mechanical Engineering, Aditya College of Engineering and Technology, Kakinada, Andhra Pradesh 533437, India*

Complete contact information is available at: https://pubs.acs.org/10.1021/acsomega.2c08164

Funding

This work is not funded by anybody or organizations.

Notes

The authors declare no competing financial interest.

REFERENCES

(1) Rismalia, M.; Hidajat, S. C.; Permana, I. G. R.; Hadisujoto, B.; Muslimin, M.; Triawan, F. Infill pattern and density effects on the tensile properties of 3D printed PLA material. *J. Phys.: Conf. Ser.* **2019**, *1402*, No. 044041.

(2) Dezaki, M. L.; Mohd Ariffin, M. K. A. The effects of combined infill patterns on mechanical properties in fdm process. *Polymer* **2020**, *12*, 1−20.

(3) Ranganathan, S., Kumar, K. S., Gopal, S., Pradeep, C. The Effect of Print Orientation and Infill Density for 3D Printing on Mechanical and Tribological Properties. In: *SAE Technical Papers*. ; 2020. doi: DOI: 10.4271/2020-28-0411

(4) Pandzic, A.; Hodzic, D.; Milovanovic, A. Effect of infill type and density on tensile properties of pla material for FDM process. *Ann. DAAAM Proc.* **2019**, *1*, 545−554.

(5) Gomes, D. C.; Nassar, E. J.; Dórea Neto, F. A.; Lima, A. E.; Martins Filho, E. F.; Oriá, A. P. Experimental acrylonitrile butadiene styrene and polyamide evisceration implant: A rabbit clinical and histopathology study. *Arq. Bras. Med. Vet. e Zootec.* **2016**, 1168.

(6) Fdm, S., Material, ABSM. *Certificate of Material Biocompatibility Certificate of Material Biocompatibility Stratasys FDM ABS M30i Material Prepared For: Stratasys*. 2019;(June):2018−2019.

(7) Santavirta, S.; Takagi, M.; Nordsletten, L.; Anttila, A.; Lappalainen, R.; Konttinen, Y. T. Biocompatibility of silicon carbide in colony formation test in vitro. A promising new ceramic THR implant coating material. *Arch. Orthop. Trauma. Surg.* **1998**, DOI: 10.1007/s004020050319.

(8) Saddow, S. E.; Frewin, C. L.; Coletti, C.; et al. Single-crystal silicon carbide: A biocompatible and hemocompatible semiconductor for advanced biomedical applications. *Mater. Sci. Forum* **2011**, 824.

(9) Heimann, R. B. Silicon Nitride, a Close to Ideal Ceramic Material for Medical Application. *Ceramics* **2021**, DOI: 10.3390/ceramics4020016.

(10) Maccauro, G., Iommetti, P. R., Manicone, P. F., Raffaelli, L. Zirconia and allumina bioceramic biocompatibility. In: *Zirconium: Characteristics, Technology and Performance*. ; 2012.

(11) Ramot, Y.; Haim-Zada, M.; Domb, A. J.; Nyska, A. Biocompatibility and safety of PLA and its copolymers. *Adv. Drug Delivery Rev.* **2016**, DOI: 10.1016/j.addr.2016.03.012.

(12) Schmitt, M, Mehta, RM, Kim, IY. Additive manufacturing experimental infill testing and optimization for automotive light-weighting. In: *SAE Technical Papers*. ; 2019. doi: DOI: 10.4271/2019-01-1275

(13) *Ceramic Composite Filament - WOL 3D - 3D Printers. WOL 3D - 3D Printers*. https://worldoflilliputs.com/product/ceramic-filament/. Published 2021. .

(14) mokereke234. (2021, April 14). *Numerical insights into tensile testing. YouTube*. https://www.youtube.com/watch?v=aug-o-DKQKY.

(15) Bhat, R.; Mohan, N.; Sharma, S.; Pratap, A.; Keni, A. P.; Sodani, D. Mechanical testing and microstructure characterization of glass fiber reinforced isophthalic polyester composites. *J. Mater. Res. Technol.* **2019**, DOI: 10.1016/j.jmrt.2019.06.003.

(16) Ma, Q.; Rejab, M. R. M.; Kumar, A. P.; Fu, H.; Kumar, N. M.; Tang, J. Effect of infill pattern, density and material type of 3D printed cubic structure under quasi-static loading. *Proc. Inst. Mech. Eng. Part C J. Mech. Eng. Sci.* **2021**, DOI: 10.1177/0954406220971667.

(17) Dave, H. K.; Patel, B. H.; Rajpurohit, S. R.; Prajapati, A. R.; Nedelcu, D. Effect of multi-infill patterns on tensile behavior of FDM printed parts. *J. Brazilian Soc. Mech. Sci. Eng.* **2021**, DOI: 10.1007/s40430-020-02742-3.

(18) Dave, H. K.; Patadiya, N. H.; Prajapati, A. R.; Rajpurohit, S. R. Effect of infill pattern and infill density at varying part orientation on tensile properties of fused deposition modeling-printed poly-lactic acid part. *Proc. Inst. Mech. Eng. Part C J. Mech. Eng. Sci.* **2021**, DOI: 10.1177/0954406219856383.

(19) Nazmul Ahsan, A. M. M.; Khoda, B. Characterizing Novel Honeycomb Infill Pattern for Additive Manufacturing. *J. Manuf. Sci Eng. Trans. ASME* **2021**, DOI: 10.1115/1.4048044.

(20) Hassan, M. R.; Jeon, H. W.; Kim, G.; Park, K. The effects of infill patterns and infill percentages on energy consumption in fused filament fabrication using CFR-PEEK. *Rapid Prototyp. J.* **2021**, DOI: 10.1108/RPJ-11-2020-0288.

(21) Bonada, J.; Pastor, M. M.; Buj-Corral, I. Influence of infill pattern on the elastic mechanical properties of fused filament fabrication (Fff) parts through experimental tests and numerical analyses. *Materials* **2021**, DOI: 10.3390/ma14185459.

(22) Karabeyoglu, S. S.; Eksi, O.; Yaman, P.; Kucukyildirim, B. O. Effects of infill pattern and density on wear performance of FDM-printed acrylonitrile-butadiene-styrene parts. *J. Polym. Eng.J Polym Eng* **2021**, DOI: 10.1515/polyeng-2021-0192.

(23) Dezaki, M. L.; Ariffin, M. K. A. M.; Serjouei, A.; Zolfagharian, A.; Hatami, S.; Bodaghi, M. Influence of infill patterns generated by cad and fdm 3d printer on surface roughness and tensile strength properties. *Appl. Sci.* **2021**, DOI: 10.3390/app11167272.

(24) Yao, Y.; Ding, C.; Aburaia, M.; Lackner, M.; He, L. A 3D weaving infill pattern for fused filament fabrication. *Int. J. Adv. Manuf. Technol.* **2021**, DOI: 10.1007/s00170-021-07694-z.

(25) Xu, H.; Wang, L.; Cao, Y.; Yu, T.; Tang, H.; Lin, J. Experimental Research of Remaining Oil Distribution for Inverted Nine-Sport Pattern and Infill Well Pattern. *Arab. J. Sci. Eng.* **2021**, DOI: 10.1007/s13369-021-06043-2.

(26) Tan, H.; Tarasov, V.; Jarfors, A. E. W.; Seifeddine, S. A design of fuzzy inference systems to predict tensile properties of as-cast alloy. *Int. J. Adv. Manuf. Technol.* **2021**, DOI: 10.1007/s00170-020-06502-4.
(27) Le, T. T. Prediction of tensile strength of polymer carbon nanotube composites using practical machine learning method. *J. Compos. Mater.* **2021**, DOI: 10.1177/0021998320953540.
(28) Huang, S.; Liu, X.; Li, D. Studies about Microstructures and Mechanical Properties of Ti(C,N) Ceramic Material Using Different Solvents. *Integr. Ferroelectr.* **2020**, DOI: 10.1080/10584587.2020.1728848.
(29) Hsueh, M. H.; Lai, C. J.; Chung, C. F.; et al. Effect of printing parameters on the tensile properties of 3d-printed polylactic acid (Pla) based on fused deposition modeling. *Polymers* **2021**, DOI: 10.3390/polym13142387.
(30) Hiroki, K.; Chrystelle, B.; Agathe, L.; Fumio, N. Tensile Properties of Mechanically-Defibrated Cellulose Nanofiber-Reinforced Polylactic Acid Matrix Composites Fabricated by Fused Deposition Modeling. *Trans. Nanjing Univ. Aeronaut. Astronaut.* **2021**, DOI: 10.16356/j.1005-1120.2021.01.006.
(31) Segun, A.; Adewuyi, B. O.; Ojo, D. O.; Gideon, O. N. Mechanical and Structural Properties of Nanocarbon Particles Reinforced in Plasticised Polylactic Acid for High Strength Application. *J. Phys. Sci.* **2021**, DOI: 10.21315/jps2021.32.2.4.
(32) Chandran, V.; Kalman, J.; Fayazbakhsh, K.; Bougherara, H. A comparative study of the tensile properties of compression molded and 3D printed PLA specimens in dry and water saturated conditions. *J. Mech. Sci. Technol.* **2021**, DOI: 10.1007/s12206-021-0415-5.
(33) Öteyaka, M. Ö.; Aybar, K.; Öteyaka, H. C. Effect of Infill Ratio on the Tensile and Flexural Properties of Unreinforced and Carbon Fiber-Reinforced Polylactic Acid Manufactured by Fused Deposition Modeling. *J. Mater. Eng. Perform.* **2021**, DOI: 10.1007/s11665-021-05694-4.
(34) Wang, Y.; Kong, D.; Zhang, Q.; Li, W.; Liu, J. Process parameters and mechanical properties of continuous glass fiber reinforced composites-polylactic acid by fused deposition modeling. *J. Reinf. Plast. Compos.* **2021**, DOI: 10.1177/0731684421998017.
(35) Yang, T. C.; Yeh, C. H. Morphology and mechanical properties of 3D printed wood fiber/polylactic acid composite parts using Fused Deposition Modeling (FDM): The effects of printing speed. *Polymers* **2020**, DOI: 10.3390/POLYM12061334.
(36) García-Cruz, H. I.; Jaime-Fonseca, M. R.; Von Borries-Medrano, E.; Vieyra, H. Extrusion parameters to produce a PLA-starch derived thermoplastic polymer. *Rev. Mex. Ing. Quim.* **2020**, DOI: 10.24275/rmiq/Poly1529.
(37) Liu, Z.; Lei, Q.; Xing, S. Mechanical characteristics of wood, ceramic, metal and carbon fiber-based PLA composites fabricated by FDM. *J. Mater. Res. Technol.* **2019**, DOI: 10.1016/j.jmrt.2019.06.034.
(38) Choudhary, N.; Sharma, V.; Kumar, P. Reinforcement of polylactic acid with bioceramics (alumina and YSZ composites) and their thermomechanical and physical properties for biomedical application. *J. Vinyl Addit. Technol.* **2021**, DOI: 10.1002/vnl.21837.
(39) Strano, M.; Rane, K.; Farid, M. A.; Mussi, V.; Zaragoza, V.; Monno, M. Extrusion-based additive manufacturing of forming and molding tools. *Int. J. Adv. Manuf. Technol.* **2021**, DOI: 10.1007/s00170-021-07162-8.
(40) Siracusa, V.; Maimone, G.; Antonelli, V. State-of-art of standard and innovative materials used in cranioplasty. *Polymers* **2021**, DOI: 10.3390/polym13091452.
(41) Singh, N.; Singh, R.; Ahuja, I. P. S.; Farina, I.; Fraternali, F. Metal matrix composite from recycled materials by using additive manufacturing assisted investment casting. *Composite Structures* **2019**, *207*, 129−135.

https://doi.org/10.1021/acsomega.2c08164
ACS Omega 2023, 8, 24786−24796